Role of Loop Residues and Cations on the Formation and Stability of Dimeric DNA G-Quadruplexes†

Mirko Cevec and Janez Plavec*

Slovenian NMR Center, National Institute of Chemistry, Hajdrihova 19, PO Box 660, SI-1001 Ljubljana, Slovenia

Received July 22, 2005; Revised Manuscript Received September 20, 2005

ABSTRACT: Formation of guanine-quadruplexes by four DNA oligonucleotides with common sequence dG_4-loop-dG_4 has been studied by a combination of NMR and UV spectroscopy. The loops consisted of 1′,2′-dideoxyribose, propanediol, hexaethylene glycol, and thymine residues. The comparison of data on modified and parent oligonucleotides gave insight into the role of loop residues on formation and stability of dimeric G-quadruplexes. All modified oligonucleotides fold into dimeric fold-back G-quadruplexes in the presence of sodium ions. Multiple structures form in the presence of potassium and ammonium ions, which is in contrast to the parent oligonucleotide with dT_4 loop. ^{15}N-filtered ^{1}H NMR spectra demonstrate that all studied G-quadruplexes exhibit three $^{15}NH_4^+$ ion binding sites. Topology of intermolecular G-quadruplexes was evaluated by NMR measurements and diffusion experiments. The spherical, prolate-ellipsoid and symmetric cylinder models were used to interpret experimental translational diffusion constants in terms of diameters and lengths of unfolded oligonucleotides and their respective G-quadruplexes. UV melting and annealing curves show that oligonucleotides with non-nucleosidic loop residues fold faster, exhibit no hysteresis, and are less stable than dimeric $d(G_4T_4G_4)_2$ which can be attributed to the absence of H-bonds, stacking between loop residues and the outer G-quartets as well as cation$-\pi$ interactions. Oligonucleotide consisting of hexaethylene glycol linkage with only two phosphate groups in the loop exhibits higher melting temperature and more negative $\Delta H°$ and $\Delta G°$ values than oligonucleotides with four 1′,2′-dideoxyribose or propanediol residues.

Guanine-rich DNA sequences can assemble into G-quartets, planar structures of four H-bonded guanines, which stack on top of each other to form G-quadruplex (*1, 2*). These sequences are found both in telomeres (*3*−*5*) and nontelomeric guanine sequences including c-*myc* oncogene (*6*), promoter region of c-*kit* oncogene (*7*), immunoglobulin switch regions (*8*), and insulin regulatory sequences (*9*), and have been used as thrombin-binding aptamers (*10, 11*) and as inhibitors of HIV integrase (*12, 13*). Telomeres are protein−DNA complexes located at the ends of chromosomes. The extreme 3′ ends of telomeres, which are single stranded and rich in guanines (e.g. 5′-TTAGGG-3′ in humans and 5′-TTTTGGGG-3′ in *Oxytricha*), have propensity to form G-quadruplex structures (*14, 15*). In normal cells telomeric DNA is shortened with each cell division (*16*). Telomerase, a ribonucleoprotein, extends 3′ DNA overhangs and thus makes cancer cells immortal (*17*). Formation of G-quadruplexes at telomere ends could in principle prevent extension of 3′ overhangs and consequently inhibit cancer cells from proliferating, which has made G-quadruplex an important target stimulating great effort in the design of small molecules that lead to their stabilization (*18*−*23*).

Spectroscopic studies on $d(G_4T_4G_4)$, oligonucleotide, which represents 1.5 repeats found in the telomere sequence of *Oxytricha nova*, have shown that it can form dimeric G-quadruplex with four G-quartets and two loops comprising four thymines spanning across the diagonal of the outer G-quartets (*24*−*27*) (Figure 1A). Orientations across glycosidic bonds around each of the four G-quartets are syn-anti-anti-syn. The 3D structure is characterized by alternating syn and anti nucleotide conformations along each strand and two pairs of adjacent parallel strands. G-quadruplex is formed only in the presence of certain cations, e.g. potassium, sodium, and ammonium ions, which are localized between or within the plane of G-quartet and reduce repulsions of four closely spaced carbonyl groups (*28*−*32*). Already a small change in the sequence can drastically affect the stability and topology of G-quadruplexes. For example, we have shown recently that $d(G_3T_4G_4)$ with 5′ terminal dG residue missing, or $d(G_4T_4G_3)$ with 3′ terminal dG residue missing with respect to $d(G_4T_4G_4)$, exhibit totally different topologies (*33*−*35*). These studies have revealed that novel folding motifs with reorientation of polarity of strands demonstrate high sensitivity on the nature of present cations.

The length of loops and details of their sequence can affect G-quadruplex stability (*11, 36*−*39*). NMR and X-ray crystal structures of $d(G_4T_4G_4)_2$ have shown that thymine residues in the loops exhibit stacking interactions and H-bonds with neighboring residues. X-ray crystal structure has demonstrated cation binding sites between the outer G-quartet and carbonyl groups of thymines (*27*). Analogous cation interac-

† This work has been supported by Slovenian Research Agency (ARRS) and the Ministry of Higher Education, Science and Technology of the Republic of Slovenia (Grant Nos. P1-0242-0104 and J1-6140-0104).

* To whom correspondence should be addressed. Phone: +386 1 47 60 353. Fax: +386 1 47 60 300. E-mail: janez.plavec@ki.si.

10.1021/bi0514414 CCC: $30.25
Published on Web 10/25/2005

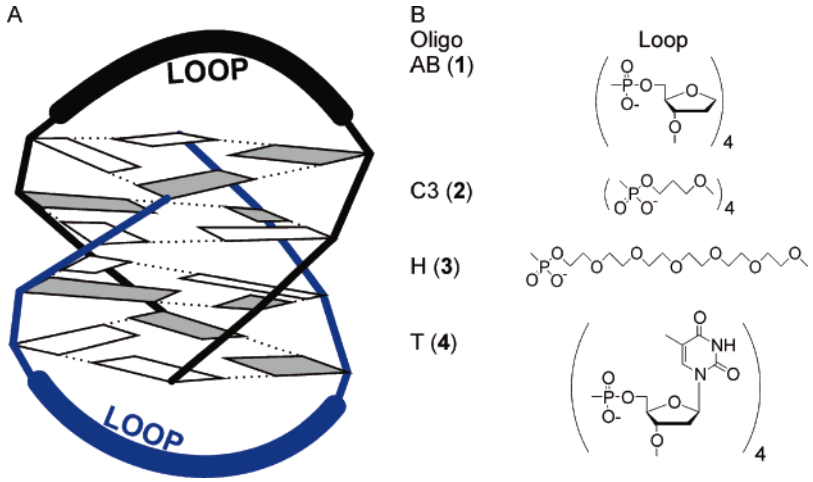

FIGURE 1: (A) Schematic presentation of the structure of $d(G_4T_4G_4)_2$. Guanine residues are presented as rectangles, where shaded rectangles indicate syn conformation. (B) Chemical structures of loop regions of oligonucleotides **1**−**4** with general formula dG_4-loop-dG_4.

tions with aromatic rings of thymine residues have not been observed under solution conditions. There are several factors that tune stability and folding process of G-rich sequences that are not fully understood. Intermolecular G-quadruplexes usually show hysteresis of melting and annealing curves (*40*−*42*), and their formation is considerably slower in comparison to intramolecular G-quadruplexes. In the present study we have focused on the influence of non-nucleosidic residues in the loop on G-quadruplex formation. We have prepared three oligonucleotides with common sequence dG_4-loop-dG_4 where loop consists of 1′,2′-dideoxyribose, propanediol, and hexaethylene glycol residues (Figure 1B) and followed their folding into G-quadruplexes by NMR and UV spectroscopy as concentration of Na^+, K^+, and $^{15}NH_4^+$ ions was increased. Modified oligonucleotides enabled us to examine the absence of base stacking interactions, different number of phosphate groups, and different length of loops on formation, stability, and structure of dimeric G-quadruplexes in comparison to the parent $d(G_4T_4G_4)$ sequence. The removal of thymine residues as in AB (**1**) demonstrated the importance of nucleobase stacking, cation interactions, and H-bonds for stability of G-quadruplexes. Additional substitution of sugar ring by noncyclic groups as in C3 (**2**) resulted in minor stabilization with respect to AB (**1**). On the other hand, the reduction of the number of the phosphate groups as in H (**3**) led to increased stability with respect to AB (**1**) and C3 (**2**). All three loop modified oligonucleotides demonstrated great sensitivity of their folding into G-quadruplexes to the nature of monovalent cations, which is in contrast to $d(G_4T_4G_4)$.

MATERIALS AND METHODS

Reagents. Oligonucleotides were chemically synthesized on an Expedite 8909 synthesizer using phosphoramidite building blocks. Coupling time for all modified residues (Glen Research) was equivalent to that used for standard nucleotides. Oligonucleotides were deprotected in concentrated aqueous ammonia at 55 °C for 12 h. DNA was purified on a 1.0 m Sephadex G25 (Sigma-Aldrich) column. Fractions containing only full-length oligonucleotides were pooled, lyophilized, redissolved in 1 mL of H_2O, and dialyzed extensively against LiCl solution. After lyophilization oligonucleotides were dissolved in 95% H_2O, 5% ^2H_2O to give 1.5−3.8 mM concentration per strand determined by UV spectroscopy at 260 nm.

NMR Measurements. NMR spectra were recorded on a Varian Unity Inova 600 MHz NMR spectrometer at 298 K. 1D ^1H NMR spectra were acquired with a 10 kHz sweep width, 32K time domain, and up to 256 scans. Water suppression was accomplished using a watergate pulse sequence. 1D ^{15}N-filtered ^1H spectra were acquired using ^{15}N decoupling during acquisition. 2D NOESY and DQF-COSY spectra were collected with 4096 complex points in the t_2 dimension, 256 increments in the t_1 dimension, and a spectral width of 10 kHz. Aliquots (2.25−5.00 μL) of 1.0 M NaCl, KCl, or $^{15}NH_4Cl$ solutions were titrated into 450 or 500 μL NMR samples and mixed thoroughly. NMR samples were thermally equilibrated in the magnet for 5−10 min before each data collection. No changes in the spectra after first data collection were observed that would indicate slow folding of **1**−**4** after increase of cation concentration by titration.

Diffusion Experiments. The translational diffusion coefficient (D_t) of a molecule in solution is inversely proportional to the translational friction coefficient (f_t) according to the Einstein−Smoluchowski equation (eq 1),

$$D_t = \frac{kT}{f_t} \tag{1}$$

where k is the Boltzmann constant and T is absolute temperature (*43*). Friction coefficients are usually calculated with the assumption that a molecule can adopt the hydrodynamic shape of a sphere, a prolate-ellipsoid, or a symmetric cylinder. The spherical model is commonly used for short duplexes or short hairpins. Friction coefficients using the spherical model are calculated by eq 2,

$$f_t = 6\pi\eta r \tag{2}$$

where η is solvent viscosity and r is hydrodynamic radius. For slightly longer nucleic acid duplexes the prolate-ellipsoid model is commonly used where f_t is defined by eq 3,

$$f_t = \frac{3}{4}\pi\eta L d^2 \frac{(1-p^2)^{1/2}}{p^{2/3}\ln\left[\frac{1+(1-p^2)^{1/2}}{p}\right]} \quad (3)$$

where L is length, d is diameter of prolate-ellipsoid, and p is defined as axial ratio d/L (*44*). Friction coefficient is according to symmetric cylinder model, which is appropriate for rodlike molecules with axial ratios from 2 to 30, defined by eq 4 (*45*).

$$f_t = 3\pi\eta \frac{L}{-\ln p + 0.312 + 0.565p - 0.100p^2} \quad (4)$$

Solvent viscosity of 95% H_2O and 5% ^2H_2O (0.903×10^{-3} kg cm^{-1} s^{-1}) was calculated from viscosities of pure solvents obtained from Lapham et al. (*46*).

Translational diffusion constants helped us to evaluate the shape and dimeric nature of oligonucleotides. Diffusion measurements were performed by spin−echo pulse sequence with gradients. The relationship between translational diffusion coefficient and NMR parameters is defined by eq 5 (*47*),

$$\ln\left(\frac{A}{A_0}\right) = -D_t(\gamma_H \delta G_z)^2\left(\Delta - \frac{\delta}{3}\right) \quad (5)$$

where A is measured intensity of NMR signal, A_0 is the highest intensity of NMR signal, γ_H is gyromagnetic ratio of proton, δ is gradient pulse duration, Δ is gradient separation time, and G_z is gradient strength. Experimental data points are plotted in the graph of $\ln(A/A_0)$ as a function of $(\gamma_H \delta G_z)^2(\Delta - \delta/3)$, and the slope is used to calculate D_t value. Measurements were performed under the following conditions: 128 scans, 1.5 s relaxation delay, 10.0 kHz sweep width, and 32K time domain. In 25 experiments the gradient strength was incremented from 0.5 to 26.1 G cm^{-1} in steps of ~1.1 G cm^{-1}, while δ (6 ms) and Δ (131.8 ms) were kept constant.

UV Melting. Temperature-dependent melting curves were measured on a Perkin-Elmer Lambda Bio 40 spectrometer equipped with a Peltier system. Oligonucleotides were dissolved in 1 mL of 50 mM NaCl and 10 mM Tris-HCl buffer at pH 7.45 and annealed by boiling for 5 min and slow cooling over several hours. After overnight incubation at 4 °C samples were placed in a stoppered quartz cuvette of 1 cm optical path length. A temperature range from 5 to 85 °C was used to monitor absorbance at 295 nm with 0.1 °C min^{-1} melting/annealing rate. Absorbance of 2′-deoxyguanosine at a wavelength of 295 nm is increased when it is involved in G-quartet (*48*). Melting points were determined by crossing point of median line between the two baselines and experimental curve. Van't Hoff thermodynamic analysis was used for all oligonucleotides assuming a two-state model. Equilibrium constants were calculated at each temperature using the relation $K_a = \alpha/2C_0(1-\alpha)$. k_{on} and k_{off} rate constants from hysteresis cycle were used in Arrhenius plots as described (*49, 50*). Extinction coefficients were calculated using nearest-neighbor model. The extinction coefficient of oligonucleotide T (**4**) is 115 200 L mol^{-1} cm^{-1}. As abasic, propanediol and hexaethylene glycol residues do not contain any groups which could absorb UV light and therefore there are no extinction coefficients available for loop residues in **1**−**3**, we have used a value of 82 200 L mol^{-1} cm^{-1} calculated for the dG_8 sequence. For comparison, the sum of extinction coefficients of two dG_4 oligonucleotides is 83 600 L mol^{-1} cm^{-1}.

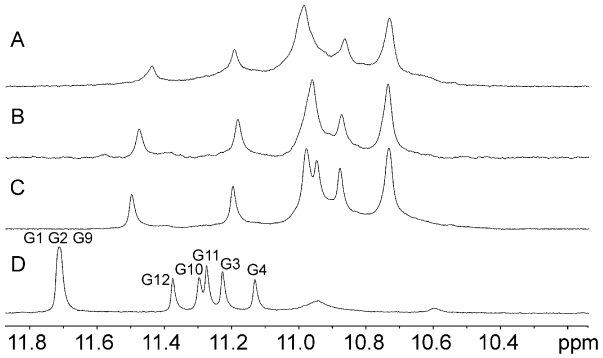

FIGURE 2: 1D ^1H NMR spectra of **1**−**4** in the presence of NaCl in 95% H_2O, 5% ^2H_2O at 25 °C. (A) AB (**1**) at 2.3 mM concentration per strand in 40 mM NaCl and pH 5.5. (B) C3 (**2**) at 1.5 mM per strand in 41 mM NaCl and pH 6. (C) H (**3**) at 3.7 mM per strand in 53 mM NaCl and pH 4.5. (D) T (**4**) at 2.0 mM per strand in 45 mM NaCl and pH 5. Imino resonances of guanines are labeled.

RESULTS

NMR Titration Experiments. Four oligonucleotides with general formula dG_4-loop-dG_4 were folded into G-quadruplex structures as concentration of monovalent cations was increased by titration of sodium, potassium, or ammonium chlorides into aqueous solutions. ^1H NMR chemical shift region of H-bonded imino protons has been particularly informative due to resonances characteristic for G-quartet formation. G-quartets with four guanine-guanine base-pairs in Hoogsteen orientation exhibit imino protons in the chemical shift range from δ10.7 to 11.7 ppm. We have noticed that loop modified G-quadruplexes adopted by AB (**1**) and C3 (**2**) exhibit five, whereas H (**3**) and T (**4**) exhibit six resolved imino resonances in the presence of Na^+ ions (Figure 2). Integration of resonances, however, revealed that G-quadruplexes adopted by oligonucleotides **1**−**4** exhibited eight imino protons, which led us to the conclusion that G-quadruplexes consisted of two or multiple of two G-quartets if the structure is symmetric. Perusal of spectra in Figure 2 shows that G-quadruplexes adopted by **1**−**3** in the presence of Na^+ ions exhibit very similar chemical shifts of their imino protons. In comparison, imino protons of G-quadruplex adopted by T (**4**) are deshielded (*25*). Similarly H8 and sugar protons for T (**4**) are deshielded with respect to **1**−**3**, which has been attributed to ring current effects of thymine residues in the loop. The aromatic nature of thymine rings in addition results in better spectral resolution of individual aromatic and sugar resonances of guanines of G-quadruplex adopted by T (**4**). G-quadruplexes adopted by **1**−**3** exhibited much poorer chemical shift separation which prevented complete resonance assignment.

Titration of oligonucleotides **1**−**3** with KCl also led to protection of imino proton resonances from exchange with bulk solution. Analysis of peaks in the range from δ10.8 to 11.8 ppm suggested that G-quadruplexes adopted by **1**−**3** in the presence of K^+ ions were characterized by eight imino H-bonded protons corresponding to the major form (Figure 3). Signals at $\delta \sim 11.7$ ppm along with other minor signals

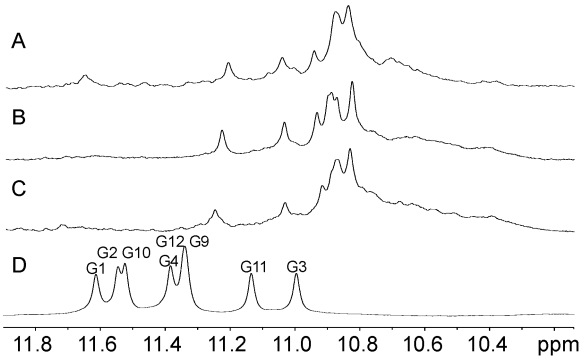

FIGURE 3: 1D ^{1}H NMR spectra of **1**−**4** in the presence of KCl in 95% H_2O, 5% ^2H_2O at 25 °C. (A) AB (**1**) at 2.3 mM concentration per strand in 20 mM KCl and pH 5.5. (B) C3 (**2**) at 1.7 mM per strand in 20 mM KCl and pH 6.5. (C) H (**3**) at 2.3 mM per strand in 5 mM KCl and pH 5. (D) T (**4**) at 3.5 mM per strand in 20 mM KCl and pH 5. Imino resonances of guanines are labeled.

indicate alternative folding of ca. 30% and 10% at 20 mM KCl for AB (**1**) and H (**3**), respectively. The comparison of ^{1}H NMR spectra in the presence of KCl and NaCl has shown that signals of imino protons are broader, which complicates their analysis. Lower concentrations of KCl (20 mM) than NaCl (40 mM) were needed to fold **1**−**3** into G-quadruplexes. Titration of oligonucleotides **1**−**3** with $^{15}NH_4Cl$ resulted in broad and poorly resolved signals. Diffusion experiments suggested that broadening was not a result of aggregation. Signal broadening was attributed to spectral overlap of several G-quadruplex structures in the presence of $^{15}NH_4Cl$ or/and to equilibrium among different structural forms that is intermediate on the NMR time scale.

Several through bond and through space NMR experiments were used to partially assign ^{1}H resonances, which enabled us to establish folding topology of G-quadruplexes. The DQF-COSY spectrum was used to identify coupled protons of deoxyribose moieties of guanine residues and to get insight into predominant sugar conformation. We could observe correlation peaks between H1′ and H2′,2″ protons, whereas correlation peaks between H3′, H4′, and H5′,5″ protons were not sufficiently resolved. The aromatic−anomeric region of 2D NOESY spectra of G-quadruplexes adopted by oligonucleotides **1**−**3** revealed four strong H8−H1′ NOE cross peaks that clearly identified four guanine bases in syn conformation. The presence of four syn residues offered evidence for the formation of a fold-back structure by **1**−**3**. It is known that T (**4**) folds into dimeric fold-back G-quadruplex with 8 syn guanine residues (4 can be observed experimentally due to the symmetric nature of the structure) in the presence of Na^+, K^+, and $^{15}NH_4^+$ ions (*30*).

We have also collected ^{15}N-filtered ^{1}H spectra of G-quadruplexes folded in the presence of $^{15}NH_4Cl$. $^{15}NH_4^+$ ions in bulk solution resonate at δ7.10 ppm. In addition, two broad signals at δ6.59 and 6.75 ppm with relative intensities of 2:1, respectively, corresponded to $^{15}NH_4^+$ ions residing inside G-quadruplexes of oligonucleotides **1**−**3**. In comparison bound $^{15}NH_4^+$ ions within G-quadruplex adopted by T (**4**) exhibit two signals with chemical shifts of δ7.31 and 7.38 ppm (*51*). Two distinct chemical shifts of bound $^{15}NH_4^+$ ions suggest that G-quadruplex structures exhibit three binding sites between four G-quartet planes. The ratio of 2:1 is due to the symmetric nature of G-quadruplex structures adopted by **1**−**4** with two ions at the outer and one at the inner

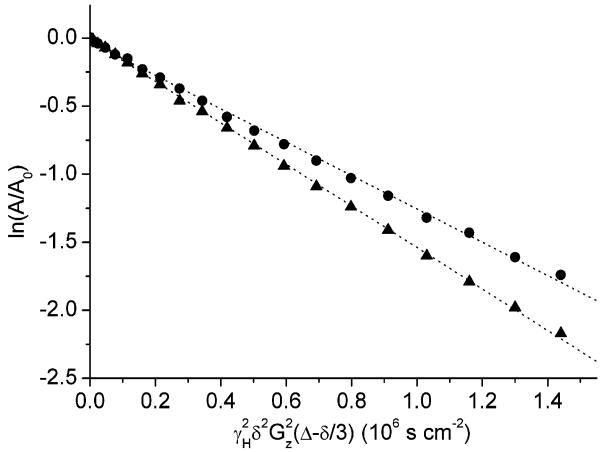

FIGURE 4: Stejskal−Tanner plot for AB (**1**) (2.3 mM per strand, pH 5.5) before addition of NaCl (filled triangle, $D_t = 1.57 \times 10^{-6}$ cm^2 s^{-1}) and at 40 mM of NaCl (filled circle, $D_t = 1.22 \times 10^{-6}$ cm^2 s^{-1}) at 25 °C.

binding site. Two issues are apparent from the comparison of ^{1}H chemical shifts of G-quadruplexes adopted by **1**−**4**. First, $^{15}NH_4^+$ ions bound at the outer and inner binding sites of G-quadruplexes with modified loops are shielded with respect to T (**4**) by $\Delta\delta$ of 0.79 and 0.56 ppm, respectively. Second, $^{15}NH_4^+$ ions at the outer binding sites experience greater chemical shift changes in the two sets of oligonucleotides due to the absence of ring current effects of thymine residues in **1**−**3**.

Protons of loop residues in G-quadruplexes adopted by **1**−**3** exhibit characteristic ^{1}H NMR spectra. H1′,1″ and H2′,2″ protons of abasic loop residues in AB (**1**) are found at $\delta \sim 4.1$ and 2.2 ppm, respectively. Two proton groups are characteristic for loop regions in C3 (**2**) with $-CH_2-$ and $-CH_2O-$ groups exhibiting chemical shifts of $\delta \sim 2.1$ and 4.1 ppm, respectively. ^{1}H NMR spectra of H (**3**) reveal a peak at $\delta \sim 3.8$ ppm corresponding to $-CH_2-$ protons which are characteristic for hexaethylene glycol linkages. We have noticed that all loop residues exhibit distinct chemical shifts when oligonucleotides **1**−**3** are single stranded and when they are folded into G-quadruplexes. Differences show that loop protons experience different chemical shielding environment upon G-quadruplex formation. However, we were not able to determine the structure of loop region or to assign groups which were spatially closer to the outside G-quartet.

Diffusion Experiments. Translational diffusion coefficients (D_t) were determined from the slopes of Stejskal−Tanner plots (Figure 4). Data in Table 1 show that unfolded oligonucleotides **1**−**3** in the absence of cations exhibit D_t values of $\sim 1.6 \times 10^{-6}$ cm^2 s^{-1}, which are very similar to the D_t value of T (**4**). The differences of $\pm 0.05 \times 10^{-6}$ cm^2 s^{-1} among unfolded **1**−**4** are in the range of experimental error. D_t values dropped by $0.2-0.4 \times 10^{-6}$ cm^2 s^{-1} upon folding of **1**−**4** into G-quadruplex structures in the presence of Na^+ ions and were between 1.2 and 1.4×10^{-6} cm^2 s^{-1} (Table 1). The comparative assessment of D_t values of folded oligonucleotides suggested that modified oligonucleotides **1**−**3** formed G-quadruplexes, which were similar in size and shape to the dimeric fold-back G-quadruplex structure adopted by T (**4**). Almost equal experimental D_t values were found in the presence of K^+ and $^{15}NH_4^+$ ions (Table S1, Supporting Information).

Table 1: Translational Diffusion Constants (D_t) and Estimated Hydrodynamic Dimensions of **1**−**4**

oligo	MW[a] (g mol^{-1})	NaCl concn (mM)	D_t[b] (10^{-6} cm^2 s^{-1})	hydrodynamic dimensions (Å)		
				spherical model[c]	cylinder model[d]	ellipsoid model[d]
AB (**1**)	3297	0.5	1.57	30.8	16.6[e]/47.7	
		40.0	1.22	39.6	24.9[e]/50.2	30.5[e]/22.7
						20.9/35.3[f]
C3 (**2**)	3129	0.5	1.61	30.0	16.6[e]/45.4	
		40.7	1.40	34.5	24.9[e]/33.8	30.5[e]/21.1
						19.5/35.3[f]
H (**3**)	2924	1.0	1.50	32.3	16.6[e]/53.0	
		53.0	1.21	40.0	24.9[e]/51.7	30.5[e]/22.8
						21.1/35.3[f]
T (**4**)	3794	1.0	1.59	30.4	16.6[e]/46.5	
		44.6	1.42	34.0	24.9[e]/32.1	30.5[e]/21.0
						19.3/35.3[f]

[a] Without counterions. [b] Error is $\pm 0.05 \times 10^{-6}$ cm^2 s^{-1}. [c] Diameter of a sphere. [d] Diameter and length are given on left and right, respectively. [e] Diameter was kept fixed in calculation of length from experimental D_t value. [f] Length was kept fixed in calculation of diameter from experimental D_t value (see text).

Subsequently experimental data were used to estimate dimensions of G-quadruplexes using spherical, prolate-ellipsoid, and symmetric cylinder models (Table 1) (*44, 45*). Dimensions of dimeric fold-back G-quadruplex structure consisting of four G-quartets were deduced initially from the known NMR (*26, 30*) and crystallographic (*27*) structures. Diameter and length of $d(G_4T_4G_4)_2$ according to the NMR structure (PDB ID 156D, (*26*)) are 24.9 and 29.7 Å, respectively. The experimental D_t value of 1.42×10^{-6} cm^2 s^{-1} for folded T (**4**) was used to calculate hydrodynamic diameter of 34 Å according to the spherical model (eqs 1 and 2). The difference between the calculated diameter (34 Å) and dimensions of the G-quadruplex adopted by T (**4**) (29.7 Å) can be attributed to the thickness of the hydration layer (2×2.2 Å). Diameters of unfolded oligonucleotides **1**−**4** were in the range from 30.0 to 32.3 Å (Table 1), which suggested that they do not adopt an extended, but rather some type of random coiled structures. Calculations using the spherical model show that folded G-quadruplexes exhibit hydrodynamic diameters between 34.0 and 40.0 Å.

According to the symmetric cylinder model single stranded (i.e. unfolded) oligonucleotides would adopt linear structure with guanine bases stacked on each other thus forming a cylinder with diameter d and length L. We have set the diameter of such a single stranded structure to 16.6 Å, which corresponds to the distance between phosphate group and aromatic moiety of guanine residue to which 2×2.8 Å (*44*) was added to account for hydration on both sides of the hypothetical linear single strand. The corresponding lengths of unfolded oligonucleotides **1**−**4** are in the range from 45.4 to 53.0 Å (Table 1), which is considerably longer than 38.5 Å (11×3.5 Å) expected for completely stacked single stranded dodecamers. Although these results are limited by several factors including imprecision in the estimate of thickness of hydration layers along the sugar−phosphate backbone and more hydrophobic aromatic side, they suggest that expected extended structure for single stranded dodecamer does not exhibit uninterrupted stacking of neighboring guanine bases. This result is in contradiction with the spherical model, which predicts more compact structure for **1**−**4** in the absence of cations.

The calculation of length of G-quadruplexes adopted by **1**−**4** using the symmetric cylinder model and experimental D_t values with the use of hydrodynamic diameter across G-quartet of 30.5 Å (24.9 Å + 2×2.8 Å) did not give a mathematically feasible solution. Exclusion of hydration layer led to reduction of diameter to 24.9 Å and resulted in the estimate of 32.1 Å for the length of G-quadruplex adopted by T (**4**), which is in reasonable agreement with 29.7 Å obtained through our simple measurements based on PDB coordinates. The diameter of dehydrated G-quartet suggested that lengths of G-quadruplexes adopted by AB (**1**), C3 (**2**), and H (**3**) are 50.2, 33.8, and 51.7 Å, respectively (Table 1). It should be noted however that the axial ratio of d/L for G-quadruplexes is below 2, which limits the applicability of the symmetric cylinder model in the case of folded **1**−**4**.

According to the prolate-ellipsoid model the estimate of hydrodynamic diameter across G-quartet of 30.5 Å (24.9 Å + 2×2.8 Å) for G-quadruplexes adopted by **1**−**4** does not give a mathematical solution to eqs 1 and 3 that would agree with experimental D_t values. If, on the other hand, the assumption is made that 30.5 Å corresponds to the long axis of the ellipsoid, short axes of ellipsoid that agree with experimental D_t values for **1**−**4** are between 21.0 and 22.8 Å (Table 1). Such a diameter, however, suggests that G-quadruplexes are compressed, which is in contradiction with known NMR and X-ray structures of $d(G_4T_4G_4)_2$. In the following step we have set the length of the prolate-ellipsoid to 35.3 Å (29.7 Å + 2×2.8 Å) and calculated the corresponding hydrodynamic diameters in the range from 19.3 to 21.1 Å (Table 1), which is ca. 10 Å smaller than the hydrodynamic diameter across G-quartet. In conclusion, the prolate-ellipsoid model did not result in dimensions of G-quadruplex structure with acceptable agreement with experimental D_t values and available high-resolution 3D structures.

We have also calculated the D_t value for G-quadruplex adopted by T (**4**) using the bead model. Hydropro program (*52*) afforded a D_t value of 1.27×10^{-6} cm^2 s^{-1} using coordinates from the NMR structure (PDB ID 156D), which is 0.15×10^{-6} cm^2 s^{-1} lower than the experimental D_t value.

UV Thermal Experiments. We have analyzed UV melting and annealing profiles of G-quadruplexes adopted by **1**−**4** in the presence of Na^+ ions. It is noteworthy that melting of G-quadruplexes adopted by oligonucleotides **1**−**4** was reversible. Oligonucleotide T (**4**), however, exhibited significant hysteresis with temperatures of half transition ($T_{1/2}$) of melting and annealing curves at 51.7 and 41.7 °C, respectively (Figure 5). Melting profiles were concentration dependent revealing (slow) intermolecular association (*53*). Arrhenius plots for G-quadruplex adopted by T (**4**) afforded activation energies for association (E_{on}) and dissociation (E_{off}) of −29 kcal mol^{-1} and 64 kcal mol^{-1}, respectively. The standard enthalpy $\Delta H°$ for the formation of G-quadruplex of T (**4**) is thus −93 kcal mol^{-1} (Table 2). Rates of association and dissociation together with thermodynamic data enabled reconstruction of the true equilibrium curve, which is shown by a dotted line in Figure 5. The experimental UV melting curve revealed a two-step dissociation for G-quadruplex adopted by T (**4**), which suggests premelting transitions in the loop region (*54*).

Melting and annealing curves for **1**−**3** were superimposable and did not display any sign of hysteresis at 0.1 °C

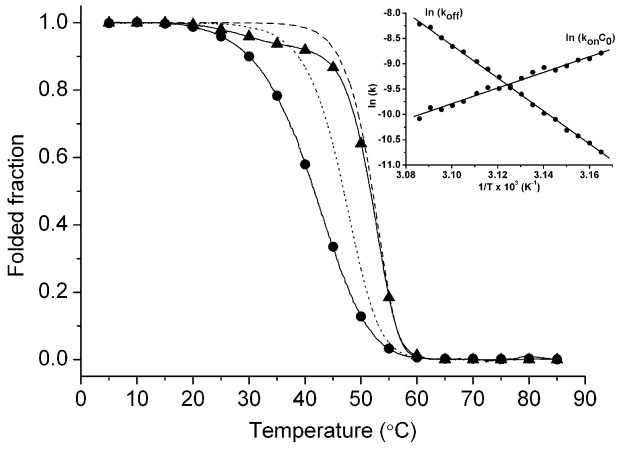

FIGURE 5: UV melting (filled triangle) and annealing (filled circle) curves for oligonucleotide T (**4**). Inset shows Arrhenius plot of ln($k_{on}C_0$) and ln(k_{off}) as a function of 1/*T*. Experimental curves are labeled only every 5 °C. Simulated melting (dashed line), annealing and equilibrium curves (dotted line) were generated with the use of the Runge−Kutta algorithm. Simulated annealing curve is perfectly superimposed with experimental values. Discrepancy between experimental and simulated melting curves indicates premelting transitions. Oligonucleotide T (**4**) was 30 μM strand concentration in 10 mM Tris-HCl buffer at pH 7.45 containing 50 mM NaCl.

Table 2: Thermodynamic Parameters for G-Quadruplexes Adopted by **1**−**4**

oligo[a]	T_m (°C)	$\Delta H°$ (kcal mol^{-1})	$\Delta S°$ (kcal mol^{-1} K^{-1})	$\Delta G°$ (25 °C) (kcal mol^{-1})
AB (**1**)	26.7 ± 0.2	−53 ± 2	−0.16 ± 0.01	−5.3 ± 0.3
C3 (**2**)	25.9 ± 0.2	−58 ± 3	−0.17 ± 0.01	−7.3 ± 0.4
H (**3**)	40.8 ± 0.2	−79 ± 2	−0.23 ± 0.01	−10.5 ± 0.3
T (**4**)[b]	46.9 ± 0.2	−93 ± 4	−0.27 ± 0.01	−12.5 ± 0.5

[a] Oligonucleotides were dissolved at ~30 μM strand concentration in 10 mM Tris-HCl buffer at pH 7.45 containing 50 mM NaCl. [b] T_m and thermodynamic parameters were estimated from simulated equilibrium curve.

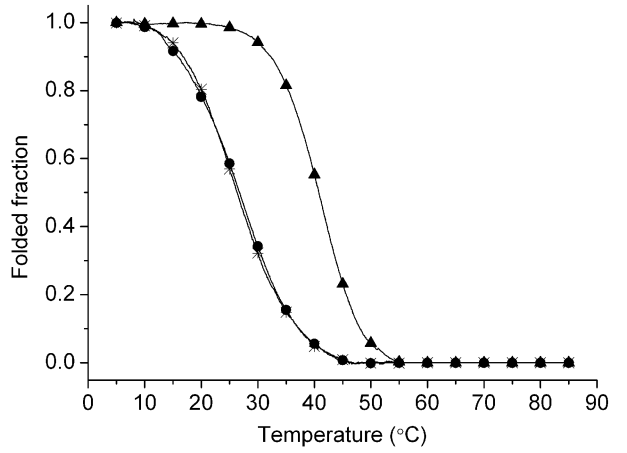

FIGURE 6: UV melting curves for oligonucleotides AB (**1**) (filled circle), C3 (**2**) (star), and H (**3**) (filled triangle). Experimental curves are labeled only every 5 °C. Melting and annealing curves are perfectly superimposed. Oligonucleotides **1**−**3** were dissolved at 30 μM strand concentration in 10 mM Tris-HCl buffer at pH 7.45 containing 50 mM NaCl.

min^{-1} melting/annealing rate (Figure 6). Analysis of UV absorbance at higher scanning speeds (up to 1 °C min^{-1}) and various oligonucleotide concentrations (from 4 to 70 μM per strand) confirmed hysteresis, whereas melting and annealing transitions were reversible for **1**−**3**. The comparison of melting curves of G-quadruplexes adopted by **1**−**4** revealed that modified oligonucleotides exhibit lower T_m values than parent T (**4**). G-quadruplexes adopted by AB (**1**) and C3 (**2**) exhibit T_m of 26.7 and 25.9 °C, respectively. In contrast T_m for G-quadruplex adopted by H (**3**) is ca. 14 °C higher (Table 2). Melting temperatures were also estimated by performing temperature-dependent ^{1}H NMR measurements in the range from 0 to 85 °C. Although signals are broad, which makes it difficult to follow chemical shift changes of individual protons as a function of temperature, we could clearly observe that melting processes were shifted to higher temperatures by over 15 °C in comparison to observations from UV spectroscopy. In addition thermodynamic parameters demonstrate that G-quadruplexes adopted by **1**−**3** are less stable than the one adopted by T (**4**) (Table 2). Examination of melting temperatures and thermodynamic data demonstrates the importance of H-bonds, stacking and cation interactions of loop thymine residues, which are absent in modified oligonucleotides for the stability of G-quadruplexes. The removal of thymine nucleobase from T (**4**) results in the reduction of $\Delta H°$ and $\Delta G°$ by 40 and 7.2 kcal mol^{-1}, respectively, as determined for G-quadruplex adopted by AB (**1**) (Table 2). The substitution of thymine residues by noncyclic propanediol groups resulted in the reduction of $\Delta H°$ and $\Delta G°$ by 35 and 5.2 kcal mol^{-1}, respectively, as can be determined from comparison of data for C3 (**2**) and T (**4**). The comparison of $\Delta H°$ and $\Delta G°$ values for H (**3**) and T (**4**) show that the former is less stable by 14 and 2 kcal mol^{-1}, respectively (Table 2). The reduction of the number of phosphate groups in H (**3**) led to increased stability with respect to AB (**1**) and C3 (**2**).

DISCUSSION

Three DNA sequences with double dG_4 runs separated by 1′,2′-dideoxyribose, propanediol, and hexaethylene glycol residues were found to fold into G-quadruplex structures in the presence of monovalent cations. Chemical shifts of imino protons and their relative integrals in ^{1}H NMR spectra suggested that oligonucleotides **1**−**3** with non-nucleosidic loops folded into single G-quadruplex structures consisting of four G-quartets in the presence of NaCl. Identification of residues with syn conformation implied formation of a fold-back structure, where syn and anti residues alternate along individual strands as has been described (*26*) for dimeric G-quadruplex structure adopted by T (**4**). NMR spectra of **1**−**3** revealed that imino, H8 and sugar resonances are compacted to a narrower chemical shift range in comparison to those of G-quadruplex adopted by the parent $d(G_4T_4G_4)$. As a consequence ^{1}H NMR spectra of modified oligonucleotides could not be completely assigned. The absence of nucleoside loop residues in G-quadruplexes adopted by **1**−**3** leads to shielding of their protons due to the lack of ring current effects of thymine residues that are stacked onto the outer G-quartets in the case of T (**4**). It is noteworthy that anisotropies of ring current effects of thymine residues in the loops of G-quadruplex adopted by T (**4**) contribute to better spectral resolution of guanine protons.

Oligonucleotides **1**−**3** were also found to fold into G-quadruplex structures in the presence of KCl or $^{15}NH_4Cl$ but did not exhibit a single set of resolved (imino) signals. We have observed differences in imino regions of ^{1}H NMR

spectra in the presence of Na^+ and K^+ ions for **1**−**4**. Different ionic radii lead to cation localization in G-quartet plane or between two neighboring G-quartets which influences interactions of cations with aromatic residues. Titration with ^{15}N isotopically labeled ammonium chloride allowed us to record ^{15}N-filtered ^1H NMR spectra, which demonstrated that G-quadruplexes adopted by **1**−**4** exhibited three $^{15}NH_4^+$ ion binding sites.

UV melting measurements showed that G-quadruplexes adopted by **1**−**3** exhibit lower melting temperatures in comparison to T (**4**) in the presence of Na^+ ions. The comparison of melting profiles established hysteresis in melting and annealing profiles of the parent oligonucleotide and its absence for modified analogues **1**−**3**. Hysteresis is correlated with slow intermolecular association which is usually observed for folding of dimeric or tetrameric G-quadruplexes. Our results indicate the importance of (non-nucleosidic) loop residues in the folding process. Oligonucleotides **1**−**3** do not contain any thymine residues in the loop and fold into G-quadruplexes faster with no hysteresis in comparison to T (**4**). The melting profile of oligonucleotide T (**4**) exhibits a biphasic shape. Slower folding of oligonucleotide T (**4**) and biphasic shape of melting profile are attributed to rearrangements in the loop region that establish stacking interactions and H-bonds. The modified oligonucleotides fold faster, but have a lower thermodynamic stability and therefore their unfolding is fast (high k_{off}). The half time of the folded species must be short compared to the parent T (**4**).

G-quadruplexes adopted by **1**−**3** are less stable than the structure of the parent T (**4**). Four residues comprise loop regions of oligonucleotides AB (**1**) and C3 (**2**). Oligonucleotide AB (**1**) incorporates four abasic residues and the same number of phosphate groups as parent oligonucleotide T (**4**). The number of bonds between G-tracts in AB (**1**) and T (**4**) is equal. The difference in $\Delta H°$ for G-quadruplexes adopted by AB (**1**) and T (**4**) is 40 kcal mol^{-1}. C3 (**2**) comprises the same number of phosphate groups and bonds as T (**4**), but no nucleobases and sugar rings in the loop. Our data show that both AB (**1**) and C3 (**2**) exhibit almost identical melting temperatures whereas enthalpies of their formation differ by 5 kcal mol^{-1}. Enthalpy of folding of T (**4**) into G-quadruplex is more negative by 40 and 35 kcal mol^{-1} than folding of AB (**1**) and C3 (**2**), respectively. Significant reduction in $\Delta H°$ and $\Delta G°$ in comparison to T (**4**) shows that base stacking inside the loop region and onto the neighboring G-quartet exhibits a great influence on G-quadruplex stability. On the other hand, G-quadruplex adopted by H (**3**) reveals greater stability than AB (**1**) and C3 (**2**). The loop in H (**3**) consists of a single hexaethylene glycol group with four bonds less than T (**4**) with additional difference in the number of phosphate groups. G-quadruplex adopted by H (**3**) contains only two phosphate groups in each loop, whereas other G-quadruplexes contain five phosphate groups. Similar correlation of stability with the number of phosphate groups in the loop has been described in the recent study by Risitano and Fox (*39*) which showed that modified intramolecular G-quadruplexes with similar length and smaller number of phosphates are more stable than their parent G-quadruplexes. The presence of nucleobases in single residue loops enhances G-quadruplex stability. Longer loops lead to destabilization if they consist of nucleobases and to stabilization if they consist of non-nucleosidic linkers (*39*). In contrast, we have found that non-nucleosidic linkers in **1**−**3** result in destabilization of G-quadruplexes which could be attributed to inter- versus intramolecular nature of G-quadruplexes in the two studies. The difference in stability between loop-modified and parent G-quadruplexes can also originate from strand directionality within G-quadruplex core, which can affect overall folding topology and not only conformation of loop residues.

Diffusion measurements show that unfolded oligonucleotides **1**−**4** exhibit similar translational diffusion constants. D_t values decreased upon addition of monovalent cations which has been attributed to folding of oligonucleotides **1**−**4** into G-quadruplexes. Three theoretical models were used to estimate diameters and lengths of unfolded and folded oligonucleotides **1**−**4**. Evaluation of D_t values by the spherical model suggested that oligonucleotides **1**−**4** were not linear single-stranded columns in the absence of cations. In the presence of K^+ and $^{15}NH_4^+$ ions oligonucleotides **1**−**4** exhibited similar experimental D_t values as in the presence of Na^+ ions, which suggested that broad ^1H NMR signals in the presence of $^{15}NH_4^+$ ions were not due to aggregation but rather due to the presence of several G-quadruplex structures. Oligonucleotides **1**−**4** exhibit very similar D_t values although molecular weights of loop modified oligonucleotides **1**−**3** are lower by 13−23%. The difference in molecular weights between oligonucleotides is apparently too small to influence their translational diffusion constants.

Studies of G-quadruplex forming capability of G-rich sequences are biologically relevant due to their (potential) roles in living organisms as well as being attractive targets for drug development. As wide biological relevance for G-quadruplex DNA is becoming more and more evident and as this motif tolerates a broad range of structural features, it is important to investigate and understand the role of residues that connect G-tracts and form loops upon folding. Previous studies have examined the effect of sequence details and length of loop on G-quadruplex stability. Our study adds to understanding of importance of stacking of loop residues between themselves and onto the neighboring G-quartets as well as number of phosphodiester functionalities. Negative charges of phosphate groups influence cation interactions with loops and within G-quadruplex core which is of primary importance for their stability and fidelity of folding process.

SUPPORTING INFORMATION AVAILABLE

^{15}N-filtered ^1H and NOESY NMR spectra (Figures S1 and S2) and translational diffusion constants in the presence of K^+ and $^{15}NH_4^+$ ions (Table S1). This material is available free of charge via the Internet at http://pubs.acs.org.

REFERENCES

1. Keniry, M. A. (2001) Quadruplex structures in nucleic acids, *Biopolymers 56*, 123−146.
2. Neidle, S., and Parkinson, G. N. (2003) The structure of telomeric DNA, *Curr. Opin. Struct. Biol. 13*, 275−283.
3. Williamson, J. R. (1994) G-quartet structures in telomeric DNA, *Annu. Rev. Biophys. Biomol. Struct. 23*, 703−730.
4. Bryan, T. M., and Cech, T. R. (1999) Telomerase and the maintenance of chromosome ends, *Curr. Opin. Cell Biol. 11*, 318−324.
5. Parkinson, G. N., Lee, M. P. H., and Neidle, S. (2002) Crystal structure of parallel quadruplexes from human telomeric DNA, *Nature 417*, 876−880.

6. Simonsson, T., Pecinka, P., and Kubista, M. (1998) DNA tetraplex formation in the control region of c-*myc*, *Nucleic Acids Res. 26*, 1167−1172.
7. Rankin, S., Reszka, A. P., Huppert, J., Zloh, M., Parkinson, G. N., Todd, A. K., Ladame, S., Balasubramanian, S., and Neidle, S. (2005) Putative DNA quadruplex formation within the human c-*kit* oncogene, *J. Am. Chem. Soc. 127*, 10584−10589.
8. Sen, D., and Gilbert, W. (1988) Formation of parallel four-stranded complexes by guanine-rich motifs in DNA and its implications for meiosis, *Nature 334*, 364−366.
9. Catasti, P., Chen, X., Moyzis, R. K., Bradbury, E. M., and Gupta, G. (1996) Structure-function correlations of the insulin-linked polymorphic region, *J. Mol. Biol. 264*, 534−545.
10. Macaya, R. F., Schultze, P., Smith, F. W., Roe, J. A., and Feigon, J. (1993) Thrombin-binding DNA aptamer forms a unimolecular quadruplex structure in solution, *Proc. Natl. Acad. Sci. U.S.A. 90*, 3745−3749.
11. Smirnov, I., and Shafer, R. H. (2000) Effect of loop sequence and size on DNA aptamer stability, *Biochemistry 39*, 1462−1468.
12. Jing, N., Marchand, C., Liu, J., Mitra, R., Hogan, M. E., and Pommier, Y. (2000) Mechanism of inhibition of HIV-1 integrase by G-tetrad-forming oligonucleotides *in vitro*, *J. Biol. Chem. 275*, 21460−21467.
13. Phan, A. T., Kuryavyi, V., Ma, J. B., Faure, A., Andreola, M. L., and Patel, D. J. (2005) An interlocked dimeric parallel-stranded DNA quadruplex: a potent inhibitor of HIV-1 integrase, *Proc. Natl. Acad. Sci. U.S.A. 102*, 634−639.
14. Kerwin, S. M. (2000) G-quadruplex DNA as a target for drug design, *Curr. Pharm. Des. 6*, 441−471.
15. Simonsson, T. (2001) G-quadruplex DNA structures—variations on a theme, *Biol. Chem. 382*, 621−628.
16. Levy, M. Z., Allsopp, R. C., Futcher, A. B., Greider, C. W., and Harley, C. B. (1992) Telomere end-replication problem and cell aging, *J. Mol. Biol. 225*, 951−960.
17. Hahn, W. C., Counter, C. M., Lundberg, A. S., Beijersbergen, R. L., Brooks, M. W., and Weinberg, R. A. (1999) Creation of human tumour cells with defined genetic elements, *Nature 400*, 464−468.
18. Zahler, A. M., Williamson, J. R., Cech, T. R., and Prescott, D. M. (1991) Inhibition of telomerase by G-quartet DNA structures, *Nature 350*, 718−720.
19. Han, H., and Hurley, L. H. (2000) G-quadruplex DNA: a potential target for anti-cancer drug design, *Trends Pharmacol. Sci. 21*, 136−142.
20. Kelland, L. R. (2000) Telomerase inhibitors: targeting the vulnerable end of cancer?, *Anti-Cancer Drugs 11*, 503−513.
21. Mergny, J. L., Lacroix, L., Teulade-Fichou, M. P., Hounsou, C., Guittat, L., Hoarau, M., Arimondo, P. B., Vigneron, J. P., Lehn, J. M., Riou, J. F., Garestier, T., and Helene, C. (2001) Telomerase inhibitors based on quadruplex ligands selected by a fluorescence assay, *Proc. Natl. Acad. Sci. U.S.A. 98*, 3062−3067.
22. Read, M., Harrison, R. J., Romagnoli, B., Tanious, F. A., Gowan, S. H., Reszka, A. P., Wilson, W. D., Kelland, L. R., and Neidle, S. (2001) Structure-based design of selective and potent G quadruplex-mediated telomerase inhibitors, *Proc. Natl. Acad. Sci. U.S.A. 98*, 4844−4849.
23. Gowan, S. M., Harrison, J. R., Patterson, L., Valenti, M., Read, M. A., Neidle, S., and Kelland, L. R. (2002) A G-quadruplex-interactive potent small-molecule inhibitor of telomerase exhibiting *in vitro* and *in vivo* antitumor activity, *Mol. Pharmacol. 61*, 1154−1162.
24. Smith, F. W., and Feigon, J. (1992) Quadruplex structure of *Oxytricha* telomeric DNA oligonucleotides, *Nature 356*, 164−168.
25. Smith, F. W., and Feigon, J. (1993) Strand orientation in the DNA quadruplex formed from the *Oxytricha* telomere repeat oligonucleotide d($G_4T_4G_4$) in solution, *Biochemistry 32*, 8682−8692.
26. Schultze, P., Smith, F. W., and Feigon, J. (1994) Refined solution structure of the dimeric quadruplex formed from the *Oxytricha* telomeric oligonucleotide d(GGGGTTTTGGGG), *Structure 2*, 221−233.
27. Haider, S., Parkinson, G. N., and Neidle, S. (2002) Crystal structure of the potassium form of an *Oxytricha nova* G- quadruplex, *J. Mol. Biol. 320*, 189−200.
28. Williamson, J. R., Raghuraman, M. K., and Cech, T. R. (1989) Monovalent cation-induced structure of telomeric DNA: the G-quartet model, *Cell 59*, 871−880.
29. Hud, N. V., Smith, F. W., Anet, F. A. L., and Feigon, J. (1996) The selectivity for K^+ versus Na^+ in DNA quadruplexes is dominated by relative free energies of hydration: a thermodynamic analysis by ^{1}H NMR, *Biochemistry 35*, 15383−15390.
30. Schultze, P., Hud, N. V., Smith, F. W., and Feigon, J. (1999) The effect of sodium, potassium and ammonium ions on the conformation of the dimeric quadruplex formed by the *Oxytricha nova* telomere repeat oligonucleotide d($G_4T_4G_4$), *Nucleic Acids Res. 27*, 3018−3028.
31. Miyoshi, D., Nakao, A., Toda, T., and Sugimoto, N. (2001) Effect of divalent cations on antiparallel G-quartet structure of d($G_4T_4G_4$), *FEBS Lett. 496*, 128−133.
32. Sket, P., Crnugelj, M., and Plavec, J. (2005) Identification of mixed di-cation forms of G-quadruplex in solution, *Nucleic Acids Res. 33*, 3691−3697.
33. Crnugelj, M., Hud, N. V., and Plavec, J. (2002) The solution structure of d$(G_4T_4G_3)_2$: a bimolecular G-quadruplex with a novel fold, *J. Mol. Biol. 320*, 911−924.
34. Crnugelj, M., Sket, P., and Plavec, J. (2003) Small change in a G-rich sequence, a dramatic change in topology: new dimeric G-quadruplex folding motif with unique loop orientations, *J. Am. Chem. Soc. 125*, 7866−7871.
35. Sket, P., Crnugelj, M., and Plavec, J. (2004) d($G_3T_4G_4$) forms unusual dimeric G-quadruplex structure with the same general fold in the presence of K^+, Na^+ or NH_4^+ ions, *Bioorg. Med. Chem. 12*, 5735−5744.
36. Balagurumoorthy, P., Brahmachari, S. K., Mohanty, D., Bansal, M., and Sasisekharan, V. (1992) Hairpin and parallel quartet structures for telomeric sequences, *Nucleic Acids Res. 20*, 4061−4067.
37. Risitano, A., and Fox, K. R. (2003) Stability of intramolecular DNA quadruplexes: comparison with DNA duplexes, *Biochemistry 42*, 6507−6513.
38. Hazel, P., Huppert, J., Balasubramanian, S., and Neidle, S. (2004) Loop-length-dependent folding of G-quadruplexes, *J. Am. Chem. Soc. 126*, 16405−16415.
39. Risitano, A., and Fox, K. R. (2004) Influence of loop size on the stability of intramolecular DNA quadruplexes, *Nucleic Acids Res. 32*, 2598−2606.
40. Wyatt, J. R., Davis, P. W., and Freier, S. M. (1996) Kinetics of G-quartet-mediated tetramer formation, *Biochemistry 35*, 8002−8008.
41. Dapic, V., Abdomerovic, V., Marrington, R., Peberdy, J., Rodger, A., Trent, J. O., and Bates, P. J. (2003) Biophysical and biological properties of quadruplex oligodeoxyribonucleotides, *Nucleic Acids Res. 31*, 2097−2107.
42. Mergny, J. L., De Cian, A., Ghelab, A., Sacca, B., and Lacroix, L. (2005) Kinetics of tetramolecular quadruplexes, *Nucleic Acids Res. 33*, 81−94.
43. Cohen, Y., Avram, L., and Frish, L. (2005) Diffusion NMR spectroscopy in supramolecular and combinatorial chemistry: an old parameter—new insights, *Angew. Chem., Int. Ed. 44*, 520−554.
44. Cantor, C. R., and Schimmel, P. R. (1980) Part II: techniques for the study of biological structure and function, in *Biophysical Chemistry*, 12th ed., pp 349−846, W.H. Freeman and Co., New York.
45. Tirado, M. M., and Garcia de la Torre, J. (1979) Translational friction coefficients of rigid, symmetric top macromolecules: application to circular cylinders, *J. Chem. Phys. 71*, 2581−2587.
46. Lapham, J., Rife, J. P., Moore, P. B., and Crothers, D. M. (1997) Measurement of diffusion constants for nucleic acids by NMR, *J. Biomol. NMR 10*, 255−262.
47. Stejskal, E. O., and Tanner, J. E. (1964) Spin diffusion measurements: spin echoes in the presence of a time-dependent field gradient, *J. Chem. Phys. 42*, 288−292.
48. Mergny, J. L., Phan, A. T., and Lacroix, L. (1998) Following G-quartet formation by UV-spectroscopy, *FEBS Lett. 435*, 74−78.
49. Rougee, M., Faucon, B., Mergny, J. L., Barcelo, F., Giovannangeli, C., Garestier, T., and Helene, C. (1992) Kinetics and thermodynamics of triple-helix formation: effects of ionic strength and mismatches, *Biochemistry 31*, 9269−9278.
50. Mergny, J. L., and Lacroix, L. (2003) Analysis of thermal melting curves, *Oligonucleotides 13*, 515−537.
51. Hud, N. V., Schultze, P., Sklenar, V., and Feigon, J. (1999) Binding sites and dynamics of ammonium ions in a telomere repeat DNA quadruplex, *J. Mol. Biol. 285*, 233−243.

52. Fernandes, M. X., Ortega, A., Lopez Martinez, M. C., and Garcia de la Torre, J. (2002) Calculation of hydrodynamic properties of small nucleic acids from their atomic structure, *Nucleic Acids Res. 30*, 1782−1788.
53. Sacca, B., Lacroix, L., and Mergny, J. L. (2005) The effect of chemical modifications on the thermal stability of different G-quadruplex-forming oligonucleotides, *Nucleic Acids Res. 33*, 1182−1192.
54. Petraccone, L., Erra, E., Esposito, V., Randazzo, A., Mayol, L., Nasti, L., Barone, G., and Giancola, C. (2004) Stability and structure of telomeric DNA sequences forming quadruplexes containing four G-tetrads with different topological arrangements, *Biochemistry 43*, 4877−4884.

BI0514414